

Pitting Corrosion Studies on Fusion Zone of Shielded Metal Arc Welded Type 316LN Stainless Steel Weldments

Srinivas Mannepalli^{1,2} · A. Ravi Shankar^{1,2} · R. P. George¹ · S. Ningshen^{1,2} · John Philip^{1,2} · G. Amarendra^{1,2}

Received: 4 March 2019 / Accepted: 5 July 2019 / Published online: 24 July 2019
© The Indian Institute of Metals - IIM 2019

Abstract During welding of 316L stainless steel (SS), heat-affected zone (HAZ) is susceptible to sensitisation and fusion zone is susceptible to pitting corrosion in stainless steel welds. High-nitrogen electrodes with 0.045–0.055 wt% C and with different Cr contents were used for welding of prototype fast breeder reactor components. As-welded and thermally aged (823 K for 2 h) weldments of type 316LN SS with different N contents made by arc welding were studied for localised corrosion. ASTM A262 Practice A and E tests and double-loop electrochemical potentiokinetic reactivation studies on as-welded and thermally aged specimens revealed the absence of sensitisation in the HAZ and in fusion zone. However, pitting potential of the weldments was found to vary with the concentration of N + Cr + Mo in fusion zone and found to be lower in the thermally aged samples. The correlation between weld microstructure, alloying elements and pitting corrosion behaviour has been discussed.

Keywords Welding · Thermal ageing · DLEPR · Pitting corrosion · Microstructures · Linear polarisation resistance (LPR)

1 Introduction

Intergranular corrosion (IGC) takes place as a result of exposure of sensitised stainless steel to a corrosive environment, and the majority of failures are reported due to weld decay during welding operation [1]. AISI type 316LN stainless steel (C = 0.02–0.03 wt% and N = 0.06–0.08 wt%) is used as a structural material for prototype fast breeder reactor (PFBR) main vessel. To improve design life from 40 to 60 years, nitrogen-enhanced type 316LN SS (N = 0.07–0.22 wt%) has been developed. Microstructural and corrosion properties of 316LN SS are evaluated, and the optimum nitrogen content for 316LN SS is found to be 0.14 wt% N [2]. Welding is unavoidable during the fabrication of PFBR components [3] and during welding operations; the heat-affected zone (HAZ) adjacent to the fusion zone is subjected to temperature exposure around 550–800 °C. Sensitisation in HAZ of austenitic stainless steel during welding is dependent on heat input, type of steel, amount of time spent in HAZ and grain size. Silva et al. [4] reported that during welding of 316L stainless steel involving different heat inputs, HAZ showed carbide precipitation [4]. Sensitisation of HAZ in the as-welded and in the thermally aged condition of austenitic stainless steels indicated the absence of sensitisation in as-welded condition, and sensitisation in HAZ increased with the increase in post-weld heat treatment time [5–9].

During the welding of stainless steels, microsegregation of alloying elements occurs [10, 11] and around 2–10% ferrite is formed for avoiding solidification cracking during welding [12–14]. Microstructural changes due to welding parameters [15] can affect the localised corrosion resistance of weldments. In austenitic stainless steel welds, microsegregation and partitioning of elements mainly depend on weld metal composition, mode of solidification

✉ R. P. George
rani@igcar.gov.in

¹ Metallurgy and Materials Group, Indira Gandhi Centre for Atomic Research, Kalpakkam, Tamil Nadu 603102, India

² Homi Bhabha National Institute, Mumbai 400094, India

and cooling rate [16, 17]. Pujar et al. [8] studied the effect of alloying elements on the pitting potential of 316N weld metal with 0.08% *N* and obtained a good correlation between Cr + Mo concentration in the matrix and pitting potential. In pitting corrosion studies on 316N weld metal with 0.07–0.13% *N*, solution-annealed condition improved pitting corrosion resistance compared to stress relieved and dimensionally stabilised conditions and attributed this to the formation of chromium carbides and sigma phase [18, 19].

Generally, the addition of nitrogen in SS retards sensitisation in the base and weld metal, and nitrogen, chromium, molybdenum in the weld improve pitting corrosion resistance [3, 20–22]. However, a systematic study on the relative resistance of 316LN SS (*N* in base material = 0.07–0.14 wt%) weldments to pitting with respect to microstructure in fusion zone and sensitisation in HAZ is still lacking, and elaborate studies are still required to provide understanding on its weldment corrosion. The present study involves systematic study on the effect of alloying elements and microstructure on pitting corrosion studies of fusion zone and sensitisation in HAZ zone of 316LN SS weldments (*N* in base material: 0.07, 0.12 and 0.14% *N*) prepared by shielded metal arc welding (SMAW) in as-welded and thermally aged condition using indigenously developed high-nitrogen electrodes with different Cr and Mo contents. Anodic polarisation and linear polarisation resistance technique (LPR) has been adopted for pitting corrosion studies and double-loop electrochemical potentiokinetic reactivation (DLEPR) technique for sensitisation evaluation. These studies will be helpful to understand the localised corrosion behaviour of weldments (in as-welded and thermally aged condition) during transit and storage of PFBR components.

2 Experimental Details

2.1 Fabrication of Weldments and Thermal Ageing

The chemical composition of the different nitrogen-alloyed 316L SS for the present study is presented in Table 1. SMAW was preferred because of its versatility, portability

and availability of electrodes that melts and produce shielding gases to prevent weld from oxidation and which are important for field applications. SMAW was adopted with modified 316N electrodes (as per AWS/ASME: SFA-5.4) of diameter 3.16 mm for the preparation of weld pads. The welding parameters employed are shown in Table 2, and the weldments were designated as 316N1, 316N2 and 316N3, respectively. Weld metal chemical composition was analysed by optical emission spectroscopy, and the results obtained are presented in Table 3.

Based on the chemical composition, mode of solidification is determined from the $\frac{Cr_{ea}}{Ni_{eq}}$ ratio in the weld metal and several authors have studied the effect of alloying elements on the weld ferrite prediction through the concept of Ni_{eq} and Cr_{eq} . Ni_{eq} considers the austenite stabilisers, whereas Cr_{eq} considers ferrite stabilisers with some potency of each element in weight percentage basis. WRC 1992 diagram shows the better prediction of ferrite that has significant Cu contents, and this diagram gives useful information between composition and mode of solidification. Delong et al. considered the effects of nitrogen on the Ni_{eq} for the better prediction of ferrite and on mode of solidification [23–25].

$$\text{Suualatas formula} = \frac{Cr_{ea}}{Ni_{eq}} = \frac{Cr + 1.37Mo + 1.5Si + 2Nb + 3Ti}{Ni + 0.3Mn + 22C + 14.2N + Cu}$$

$$\text{Delongs formula} = \frac{Cr_{ea}}{Ni_{eq}} = \frac{Cr + Mo + 1.5Si + 0.5Nb}{Ni + 0.5Mn + 30(C + N)}$$

$$\text{WRC 1992 formula} = \frac{Cr_{ea}}{Ni_{eq}} = \frac{Cr + Mo + 0.7Nb}{Ni + 0.25Cu + 35C + 20N}$$

Liquid penetrant and radiographic examinations were performed on the weld pads to check defects and porosity that occurred during welding. For IGC studies, weldment with 100 × 10 × 3 mm dimensions and for DLEPR and polarisation studies, weldments with 17 × 10 × 10 mm dimensions were machined out. Fusion zone samples were also studied for pitting corrosion. 823 K for 2 h represents dimensional stabilisation heat treatment, and hence, the present study is useful to understand the effect of

Table 1 Chemical composition of nitrogen-alloyed 316LN SS in wt%

Alloy heat	N	C	Mn	Cr	Mo	Ni	Si	S	P	Fe	Microhardness of BM (VHN)
316LN1	0.07	0.027	1.76	17.53	2.49	12.2	0.22	0.0055	0.013	Bal	155.3
316LN2	0.11	0.030	1.78	17.62	2.51	12.27	0.21	0.0055	0.015	Bal	174.4
316LN3	0.14	0.025	1.74	17.57	2.53	12.15	0.20	0.0041	0.017	Bal	185.7

Table 2 The welding parameters employed during welding

SMAW-welded 316LN SS	No. of passes	Arc current (A)	Arc voltage (V)	Welding Speed (mm/min)	Heat input (KJ/mm)	Microhardness in HAZ (VHN)
316N1	5	80	25.3	107	0.87	170–180
316N2	5	82.5	25	110.5	0.86	192–208
316N3	6	120	25	100	1.32	205–230

Table 3 Chemical composition of the weld metals, in wt%

Weldment identity	N	C	Mn	Cr	Mo	Ni	Si	Fe
316N1	0.07	0.052	1.65	17.17	1.1	11.62	0.46	Bal
316N2	0.08	0.050	1.65	18.07	2.0	11.47	0.47	Bal
316N3	0.10	0.050	1.65	19.0	2.3	11.73	0.32	Bal

dimensional stabilisation heat treatment on the corrosion behaviour during storage of PFBR components. Figure 1 shows schematic of the weld pad showing locations from where specimens were extracted and used for pitting corrosion and sensitisation studies. Figure 2 shows fusion zone, HAZ (zone where grain growth occurs) and the base metal of the three weldments.

2.2 Characterisation of Welds

Ferritoscope was used for the measurement of delta ferrite over weldments were polished up to 1 μm diamond finish. Nearly 25 measurements were done on the weld metal at different locations in the thickness direction. The average value of delta ferrite in terms of ferrite number was reported. The ferrite number measurements within fusion

zone and on the top of the bead and in thermally aged condition were also carried out. These results are presented in Table 4.

Weldments were polished up to 1 μm finish and 10% oxalic acid was used during electrolytic etching and etching was carried out at 2 V for 20 s in order to reveal microstructures of weld zone by using optical microscopy [26]. Modified Murakami reagent test [27] was conducted at 353 K (20 g KOH + 20 g $\text{K}_3\text{Fe}(\text{CN})_6$ in 100 ml of H_2O) for 90 s on the as-welded specimen and thermally aged specimens were polished up to 1 μm diamond finish followed by chemical etching for phase identification.

The grain size at different regions of HAZ from the weld fusion line was determined after electrolytic etching at 6 V using nitric acid (60 ml) and water (40 ml) by linear intercept method [28]. Microhardness measurements were conducted from base metal to fusion zone using microhardness tester of 500 g load with a dwell time of 15 s, and three measurements were done at each point and the average value is shown in Tables 1 and 2. X-ray diffraction (XRD) studies were carried out on the weld material with INEL X-ray diffractometer with $\text{Co } K_\alpha$ (1.787 \AA) source for identification of phases.

2.3 Intergranular Corrosion Studies

Electrolytic etching of weldments polished up to 1 μm mirror finish was carried out at 1 A/cm^2 for 5 min using 10 wt% ammonium persulphate to reveal microstructures at different regions of HAZ. Classification of microstructures, i.e. step, dual, ditch, was done as per ASTM A262 Practice A test [29]. ASTM A262 Practice E test was conducted as per the procedure mentioned in ASTM A262-14 standard [29] on the weldments with dimensions

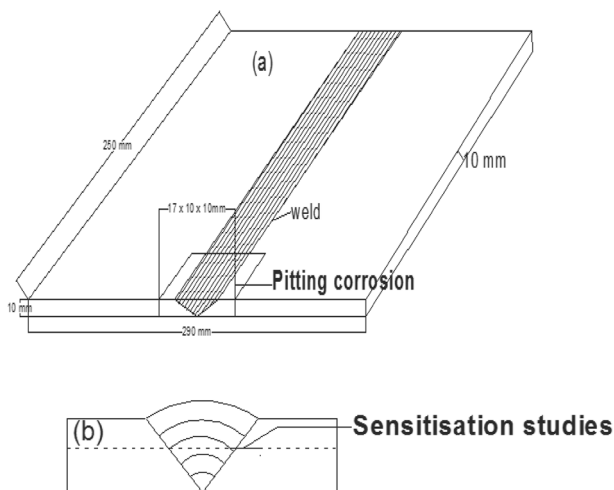


Fig. 1 a Schematic of weld pad showing weldment sample used for pitting corrosion studies and b cross-sectional view showing location for sensitisation studies

Fig. 2 Optical micrographs obtained on as-deposited weldments showing fusion, HAZ, base metal **a** 316N1, **b** 316N2, **c** 316N3

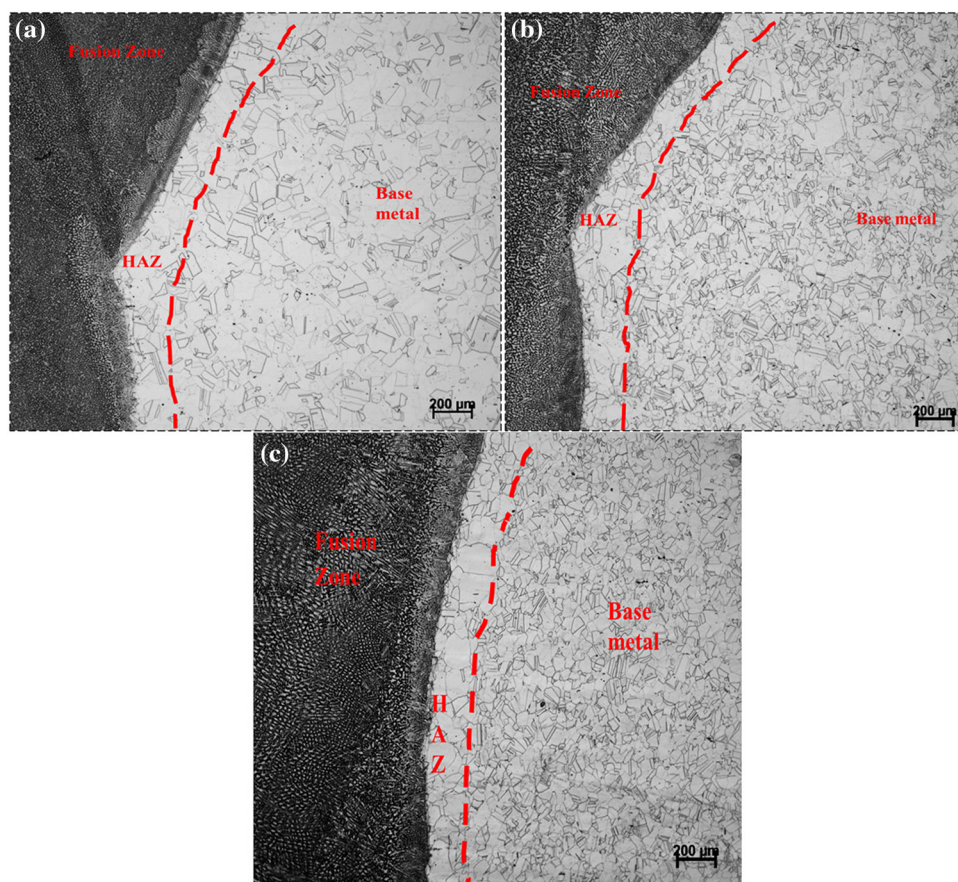


Table 4 Ferrite number measurements obtained for 316N SS weld-metal (in as welded and in thermally aged condition) using calibrated ferritoscope

Sample	Average value	On the top of bead
316N1	5.53	5.0
316N2	6.17	5.3
316N3	2.9	2.8
Thermally aged 316N1	4.5	3.7
Thermally aged 316N2	5.0	4.6
Thermally aged 316N3	1.7	2.0

100 × 10 × 3 mm in the as-welded condition polished up to 320 grit finish followed by bend test to observe cracks for IGC susceptibility.

As-welded condition and thermally aged condition specimens with 17 × 10 × 10 mm were mounted and polished up to 1 µm mirror finish. DLEPR test was conducted in acidified ammonium thiocyanate solution, i.e. 0.5 M H₂SO₄ + 0.01 M NH₄SCN solution. DLEPR test was carried out in two steps: (1) polarising the specimen at − 0.5 V (Ag/AgCl) for 120 s and (2) anodically polarising the specimen from − 0.5 to 0.3 V (Ag/AgCl) and from 0.3

to − 0.5 V (Ag/AgCl) at the scan rate of 1.6 mV/s. Degree of sensitisation (DOS) was calculated from the ratio of I_r/I_a where I_r is reactivation current and I_a is activation current.

2.4 Potentiodynamic Polarisation Studies

The anodic polarisation experiments were performed on weldment and fusion zone specimens both in as-welded and thermally aged condition polished up to 1 µm diamond finish at ambient temperature in the acidic chloride electrolyte of 0.5 M H₂SO₄ + 0.5 M NaCl solution with Ag/AgCl as a reference electrode, platinum foil as the counter electrode. For deaeration purpose, purging was carried out with argon gas for 1 h. Similarly, experiments were also carried out on as-welded and thermally aged samples in 0.5 M H₂SO₄ and 0.5 M NaCl separately under the same experimental condition. After stabilising the open circuit potential for 45 min, anodic polarisation studies were carried out by sweeping the potential from − 0.5 to 1.2 V (Ag/AgCl) at a scan rate of 0.1667 mV/s. In the present study, the potential at which the anodic current was 2.5×10^{-5} A/cm² was considered as critical pitting potential E_{pit} [8]. Anodic polarisation was stopped when the current reached a maximum value of 10^{-3} A/cm². In

order to examine the initiation sites for pits, the polarised specimens with pits were electrolytically etched in 10% ammonium persulphate at 1 A/cm² cleaned, dried and observed in the optical microscope and scanning electron microscope (SEM).

In order to determine polarisation resistance, fusion zone specimens with an area of 0.6 cm² were polished up to 1 μm diamond finish and then linear polarisation resistance experiments (LPR) were carried out in 0.5 M H₂SO₄ + 0.5 M NaCl solution. For deaeration purpose, argon gas was purged for 1 h. LPR experiments involved two steps: (1) recording specimen OCP potential for 45 min and (2) potential sweep of ± 0.02 V (Ag/AgCl) around corrosion potential at a scan rate of 0.1667 mV/s. Current density vs voltage graph was recorded from which polarisation resistance was determined.

3 Results and Discussions

3.1 Mode of Solidification, Microstructure and Ferrite Number

Using the chemical composition of weld metal, $\frac{Cr_{eq}}{Ni_{eq}}$ ratio has been calculated for 316N1, 316N2 and 316N3 and the ratios are tabulated in Table 5. Since two formulae shows $\frac{Cr_{eq}}{Ni_{eq}}$ in all the weldments less than 1.5, the mode of solidification for the weld metals is austeno-ferritic (AF mode) [18]. Ferrite content in the weld is dependent on many factors such as composition, solidification rate, cooling rate, dissolution of ferrite, ferrite morphology, etc. [30]. The average ferrite number obtained is 5.53 in case of 316N1 weld, whereas it is 6.17 and 2.93 in case of 316N2 and 316N3 weld, respectively, which is in the range of 3–7 and in thermally aged condition it decreases. Ferrite number in the range of 3–7 is required to avoid hot cracking in the weldments [3]. In the present study, 316N1, 316N2 and 316N3 weld metals are solidified with austeno-ferritic mode with intercellular ferrite. Figure 3 shows the microstructures of 316N welds obtained in the oxalic acid etch test at 2 V. The microstructures in the 316N1, 316N2 and 316N3 welds show vermicular morphology, isolated

globules and continuous stringers of ferrite at cellular boundaries. The weld metals which solidifies as austeno-ferritic mode structures are cellular in nature with inter-cellular ferrite and vermicular morphology, elongated in the heat flow direction with ferrite across cell boundaries [31].

Figure 4 shows the microstructures of 316N welds etched in modified Murakami solution. The microstructures reveal carbides (black), sigma phase (blue) and ferrite (yellow–brown) colouration. Globular morphology of ferrite is observed in 316N3 weld metal microstructure as shown in Fig. 4d due to solidification mode [31] and also thermal effects during welding [14]. As shown in Table 6, sensitisation is not observed in the weld during multipass welding. It is a well-known fact that the transformation of delta ferrite to carbide is dependent on the carbon content and temperature. In this study, microstructure of 316N1, 316N2 and 316N3 weldments after thermal ageing (823 K/ 2 h) (Fig. 5) reveals carbides that were formed due to the dissolution of ferrite. In the present study, XRD studies have also been carried out to provide a better understanding of the identification of phases. XRD studies as shown in Fig. 6 shows austenite and ferrite peaks; however, carbide precipitation is not detected in the XRD result indicating inadequate volume fraction of carbide for estimation in XRD. Further, Parvathavarthini et al. [26] and Pujar et al. [18] have also reported the presence of carbide precipitates after heat treatment at 823 K. In the present study, microstructural phases have been characterised qualitatively to reveal the differences in the concentration of elements between phases and identification of chromium carbide precipitation. Figure 7a–c shows the EDS spectra obtained on the austenite phase along with chromium-rich carbide precipitates. In Fig. 7a–c, spectrum acquired from the carbide precipitate and austenite shows Cr enrichment and depleted Ni in carbide, whereas austenite matrix shows Ni enrichment with depleted Cr. These results are in good agreement as reported by Ghosh et al. [32]. SEM EDS spectra on austenite and chromium carbide phases indicates that carbide phase is enriched with Cr and depleted in Ni compared to austenite [32].

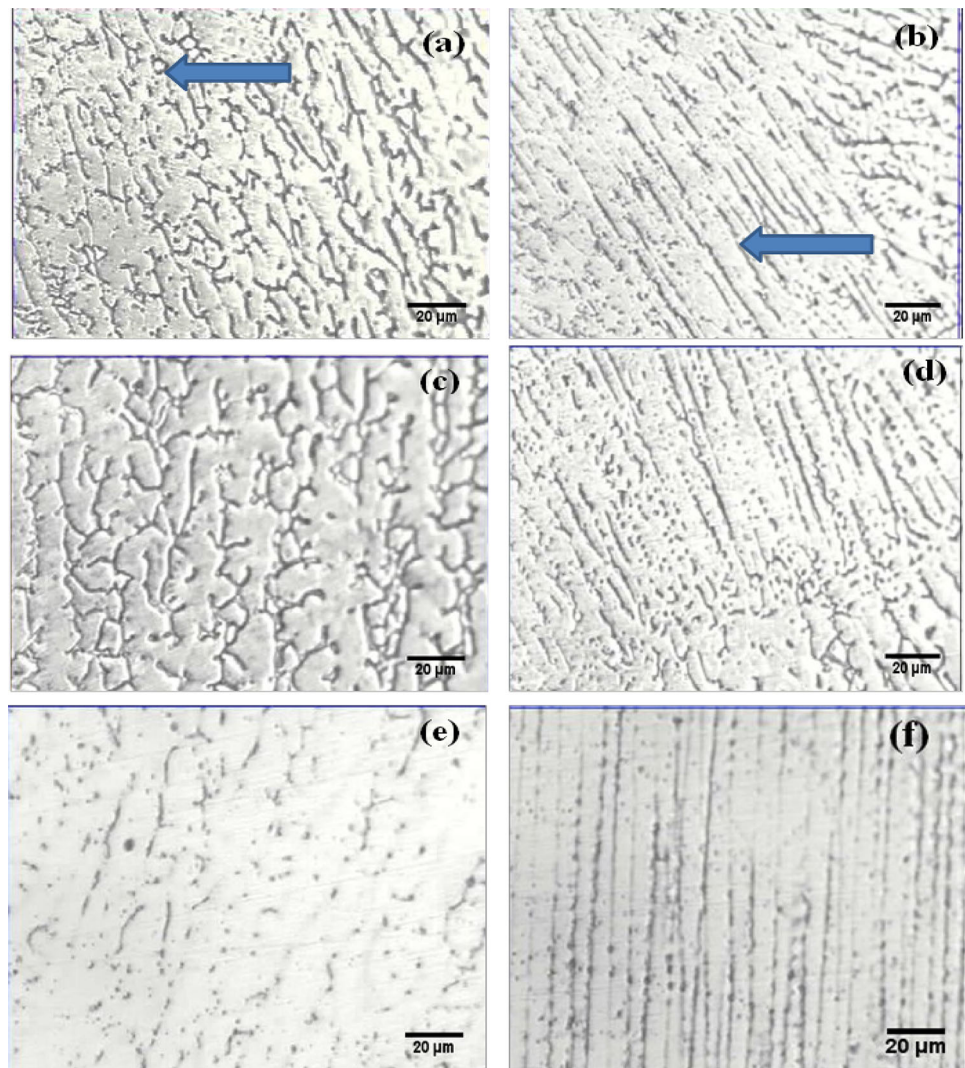
3.2 Intergranular Corrosion Studies

The average grain sizes of HAZ of 316N1, 316N2 and 316N3 have been found to be 55.44 ± 6 μm, 57.7 ± 2 μm and 68 ± 2 μm, respectively, in the HAZ compared to the three base metals (316LN1: 43 ± 2 μm; 316LN2: 54 ± 5 μm; and 316LN3: 60 ± 6 μm). Figure 8 shows the optical micrographs obtained after ASTM A262 Practice A test at different HAZs of the weldments of 316N3, 316N2 and 316N1. Step structure is clearly evident in different HAZs of 316N1, 316N2 and 316N3 weldment,

Table 5 Cr_{eq}/Ni_{eq} ratio for weld metals

Name of material	Cr _{eq} /Ni _{eq} ratio		
	Suataalas formula	Delongs formula	WRC 1992 formula
316N1	1.32	1.16	1.23
316N2	1.47	1.22	1.36
316N3	1.5	1.46	1.40

Fig. 3 Optical micrographs of microstructures obtained by etching in oxalic acid for **a**, **b** 316N1, **c**, **d** 316N2 and **e**, **f** 316N3 weld metal showing vermicular morphology, isolated globules and continuous stringers of ferrite. Arrows in **a** indicates vermicular, and arrow in **b** indicates continuous stringers



indicating that carbide precipitation is absent; thus, sensitisation is minimum. Studies on type 316L SS indicate that DLEPR is an effective technique that can distinguish step, dual and ditch structure. Aydogdu et al. [33] carried out a detailed study on the effect of different parameters on DLEPR curves on 316L SS and reported that DLEPR value between 0 and 0.1% corresponds to step structure, and 0.2–2% corresponds to the dual structure. The absence of reactivation current in Table 6 compliments the step structure as evident in optical micrographs (Fig. 8). Sensitisation evaluation carried out using ASTM A262 Practice E responds only when Cr-depleted zones due to carbides are less than 12% Cr followed by U bend in uniaxial condition (for IGC) for the observation of cracks in the U bend region [29, 34]. Weldments (316N1, 316N2 and 316N3) after conducting U bend test shows the absence of cracks in HAZ, and hence, the possibility of IGC is ruled out. Studies carried out by Parvathavarthini et al. [35] on nitrogen-alloyed 316L SS indicated that

nitrogen increases the time required for sensitisation in time–temperature sensitisation diagrams (TTS) and at 948 K (nose temperature), the time required for sensitisation is 16–24 h [35].

In the present study, there is a small variation in grain size in HAZ. Microhardness increases from base metal to HAZ, as shown in Tables 1 and 2 for all the three welds, and the presence of some ferrite around 0.2–0.4 FN is observed. It is important to note that although there is an increase in grain size in 316N3 HAZ compared to 316N1 HAZ and 316N2 HAZ, microhardness increases in 316N3 HAZ due to the presence of high-nitrogen and residual stresses created during welding [14]. Thus, in the present study, 316LN SS HAZ shows step structure due to a small variation in grain size and high nitrogen in 316L SS. Nitrogen plays an important role in HAZ as it increases the time required for sensitisation. Type 316LN SS and grain sizes in HAZ increase the time required for sensitisation. Sensitisation is dependent on the thermodynamics and

Fig. 4 Optical micrographs of microstructures obtained by etching in modified Murakami reagent for weld zone showing vermicular ferrite in **a** 316N1, **b** 316N2 and **c** 316N3 and globular morphology in (316N3) **(d)**

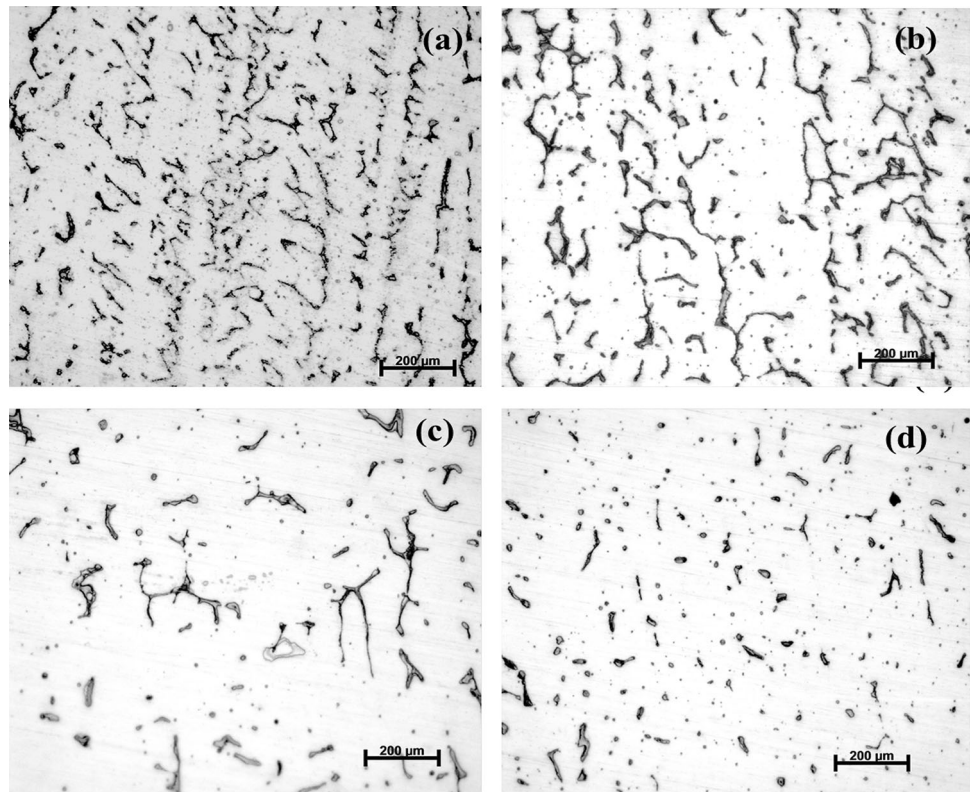


Table 6 DLEPR results for 316N weldments

Sample	% Degree of sensitisation, DOS		
	I_a (A/cm ²)	I_r (A/cm ²)	DOS (I_r/I_a)
316N1	0.021	1.7×10^{-6}	8.5×10^{-5}
316N2	0.0032	–	–
316N3	0.0063	–	–
Thermally aged 316N1	0.02	2.6×10^{-5}	8.5×10^{-3}
Thermally aged 316N2	0.0067	–	–
Thermally aged 316N3	0.0059	–	–
316N1 HAZ	0.0057	–	–
316N2 HAZ	0.0110	–	–
316N3 HAZ	0.0220	–	–

kinetics of carbide precipitation. Thermodynamically, carbide precipitation is feasible at 873–1073 K, and kinetics of carbide precipitation is dependent on chromium diffusion. Since chromium diffusion is very slow and welding conditions normally will not take longer time, chromium carbide precipitation is difficult to occur during welding conditions [1].

Silva et al. [4] reported carbide precipitation 316L SS HAZ during welding operations involving heat input and presence of ferrite in HAZ, and he attributed this to

chromium and nickel partitioning that reaches the temperature of austenite/delta ferrite. Effect of nitrogen on 304 and 316L SS indicate that nitrogen is beneficial from sensitisation point of view up to 0.14 wt% N [36].

3.3 Pitting Corrosion Studies

Figure 9a shows anodic polarisation curves of 316N weld metal and thermally aged 316N weld metal obtained in 0.5 M H₂SO₄ solutions. It is observed that there is not

Fig. 5 Optical micrographs of microstructures obtained by modified Murakami etching test of thermally aged weld metal **a** 316N1, **b** 316N2 and **c** 316N3 showing the presence of carbides (arrow mark)

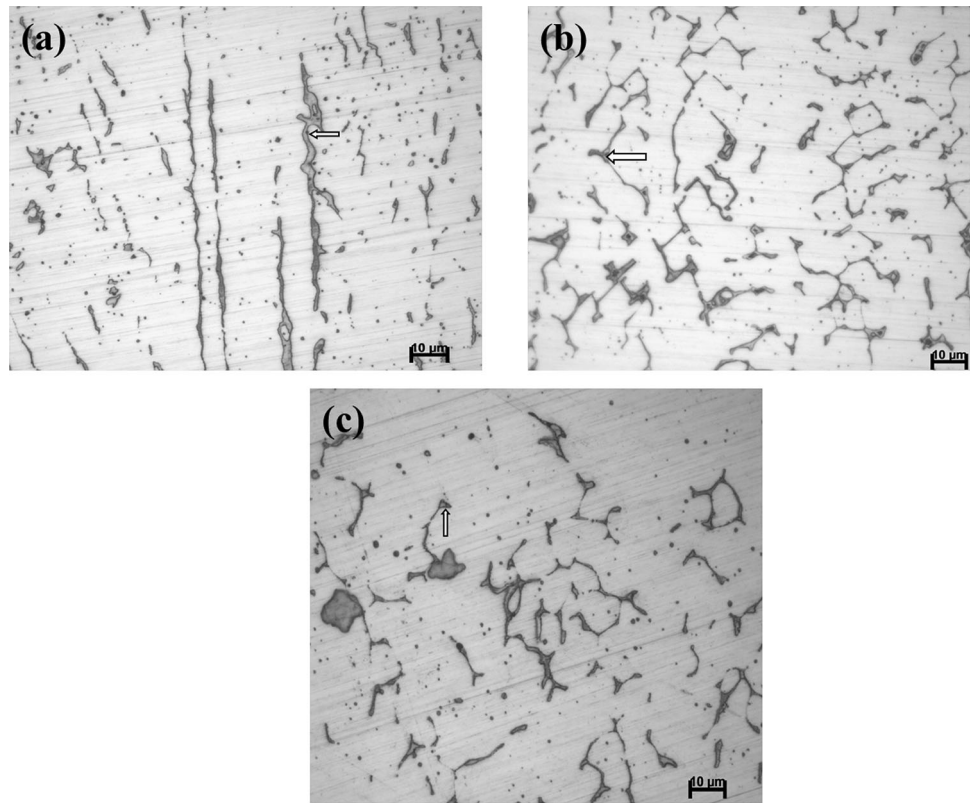


Fig. 6 XRD obtained on thermally aged weld metal **a** 316N1, **b** 316N2 and **c** 316N3 showing the presence of austenite and ferrite

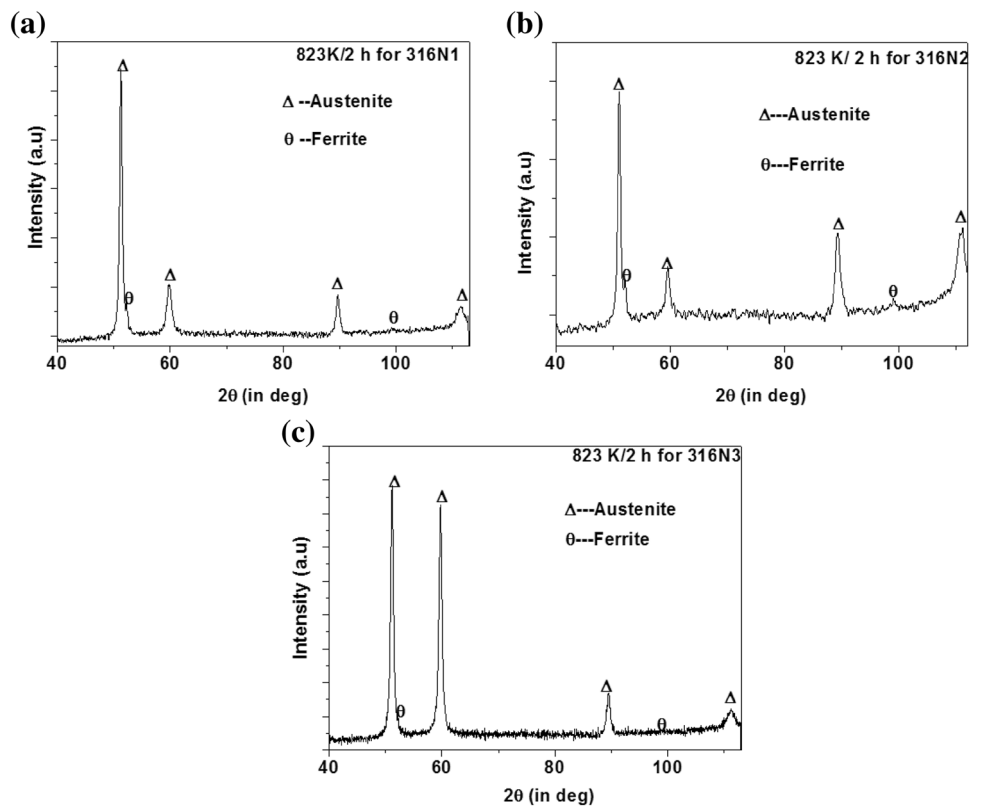
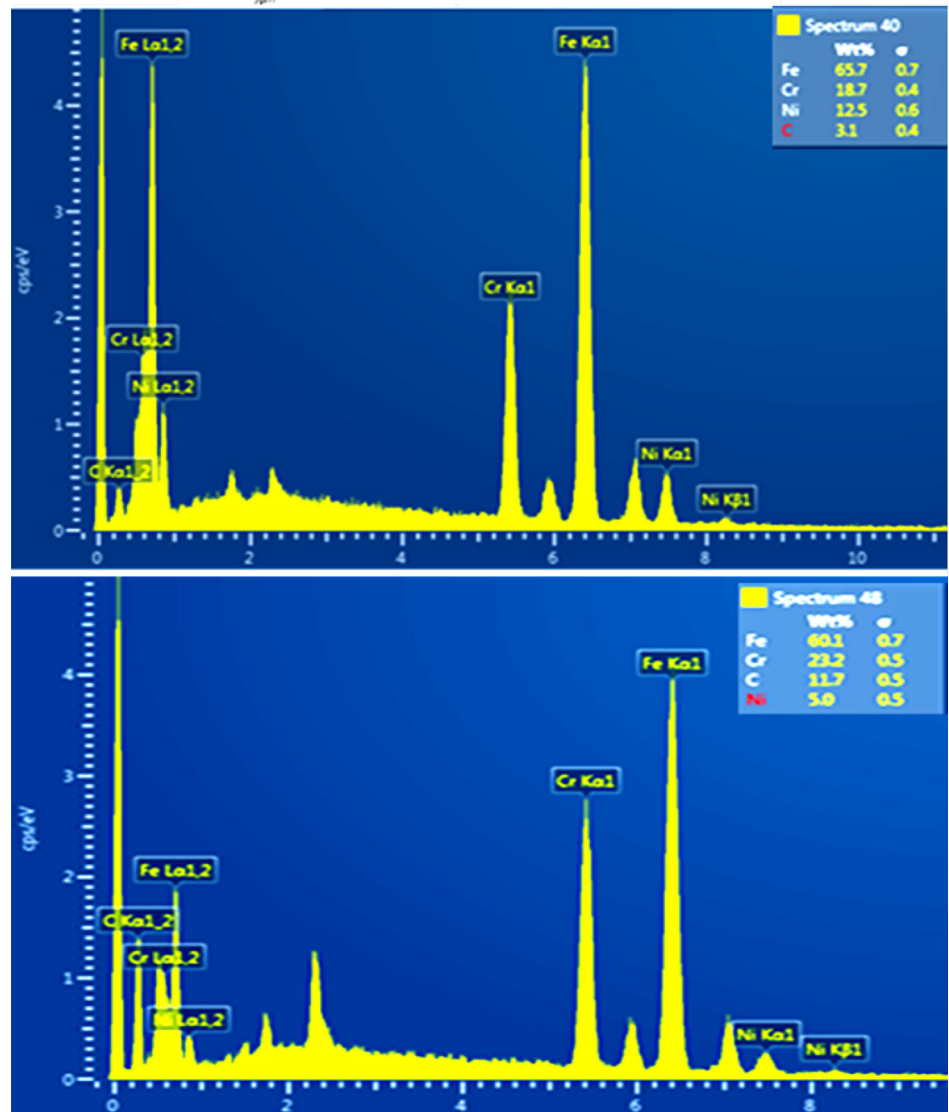
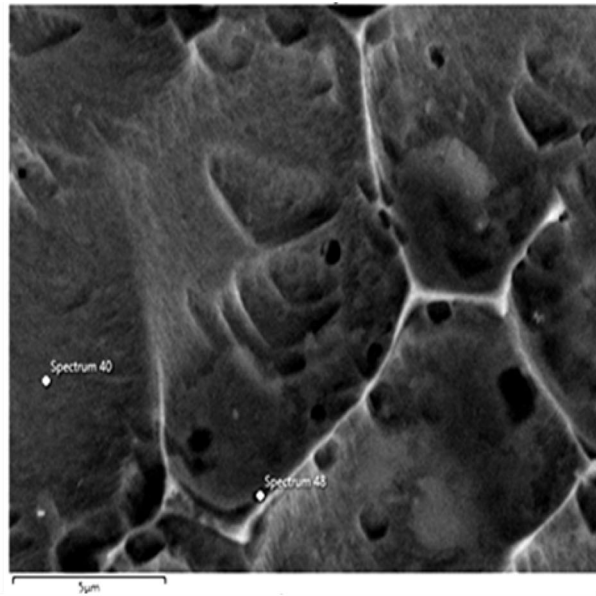


Fig. 7 a SEM EDS spectra obtained on thermally aged 316N1 showing the presence of austenite (spectrum 40) and chromium carbide (spectrum 48). **b** SEM EDS spectra obtained on thermally aged 316N2 showing the presence of austenite (spectrum 24) and chromium carbide (spectrum 18). **c** SEM EDS spectra obtained on thermally aged 316N3 showing austenite (spectrum 14) and chromium carbide (spectrum 15)

(a)



(b)

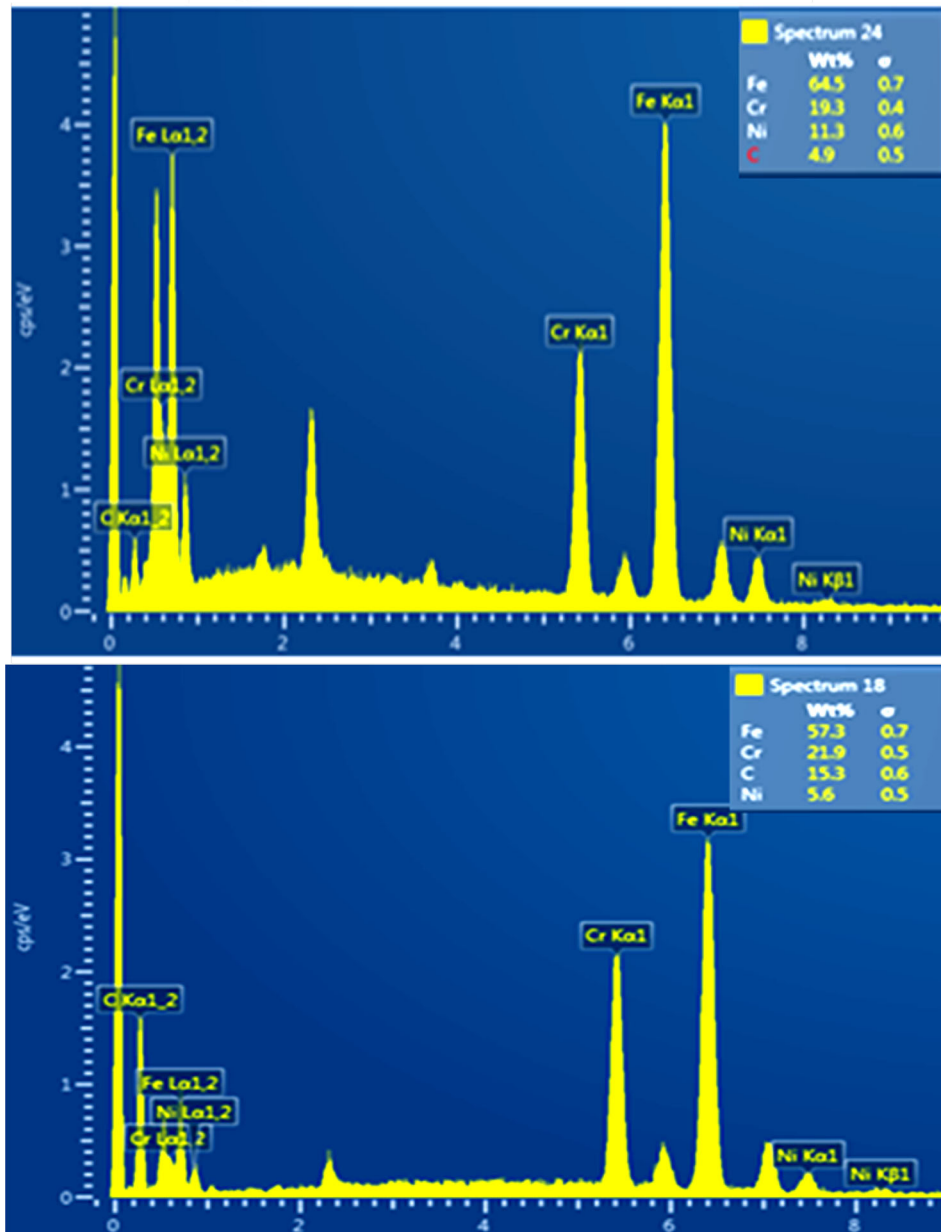
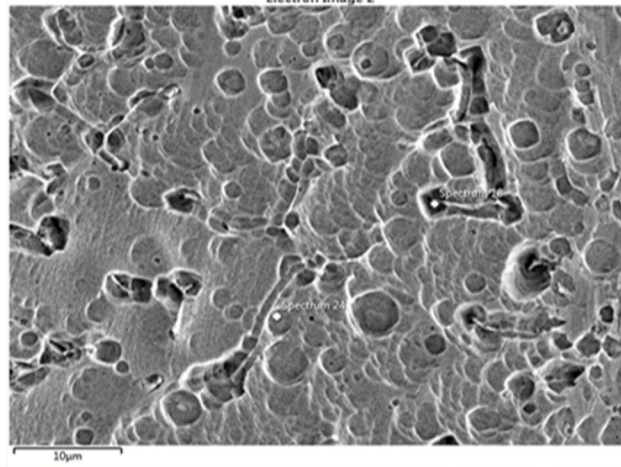


Fig. 7 continued

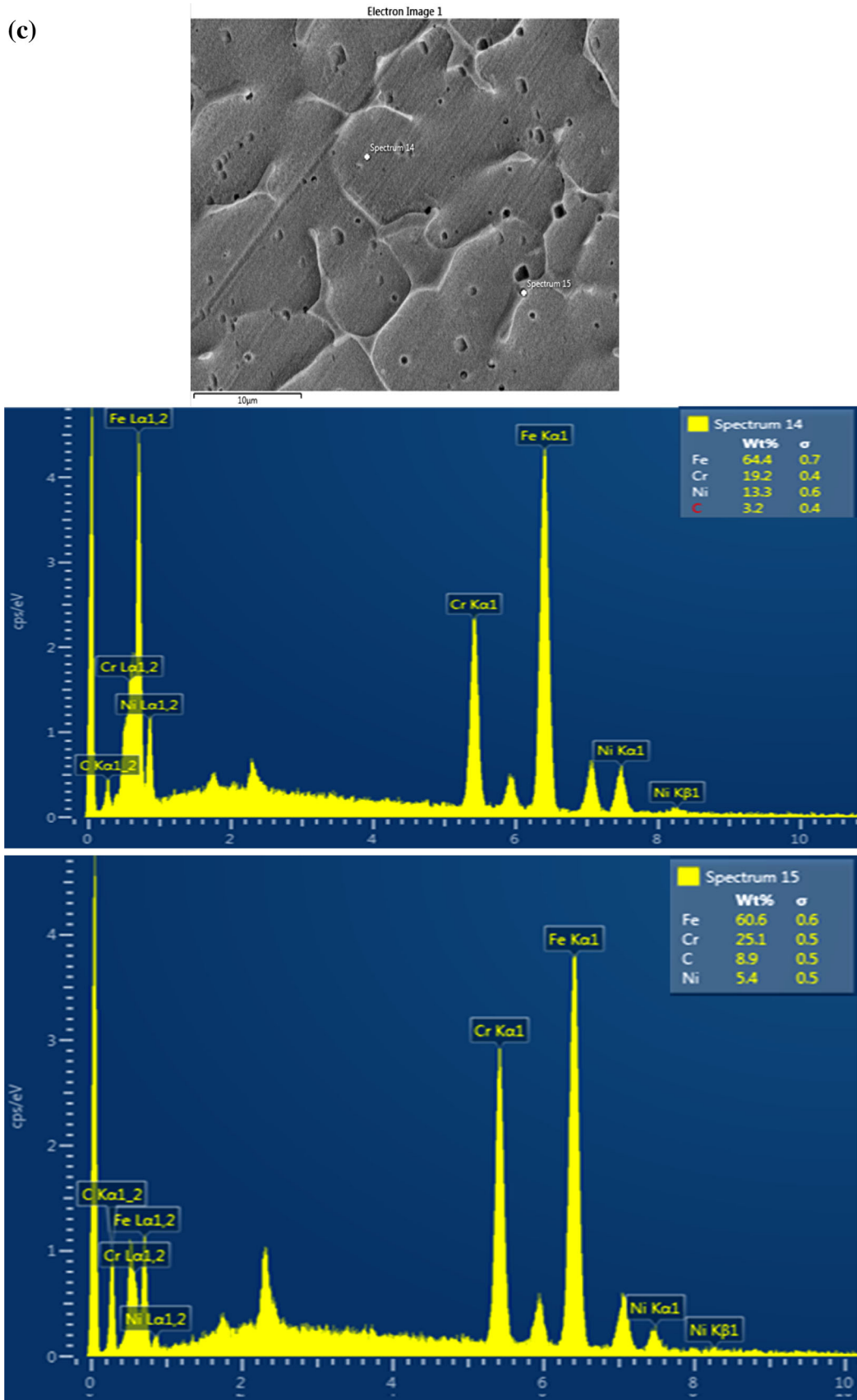


Fig. 7 continued

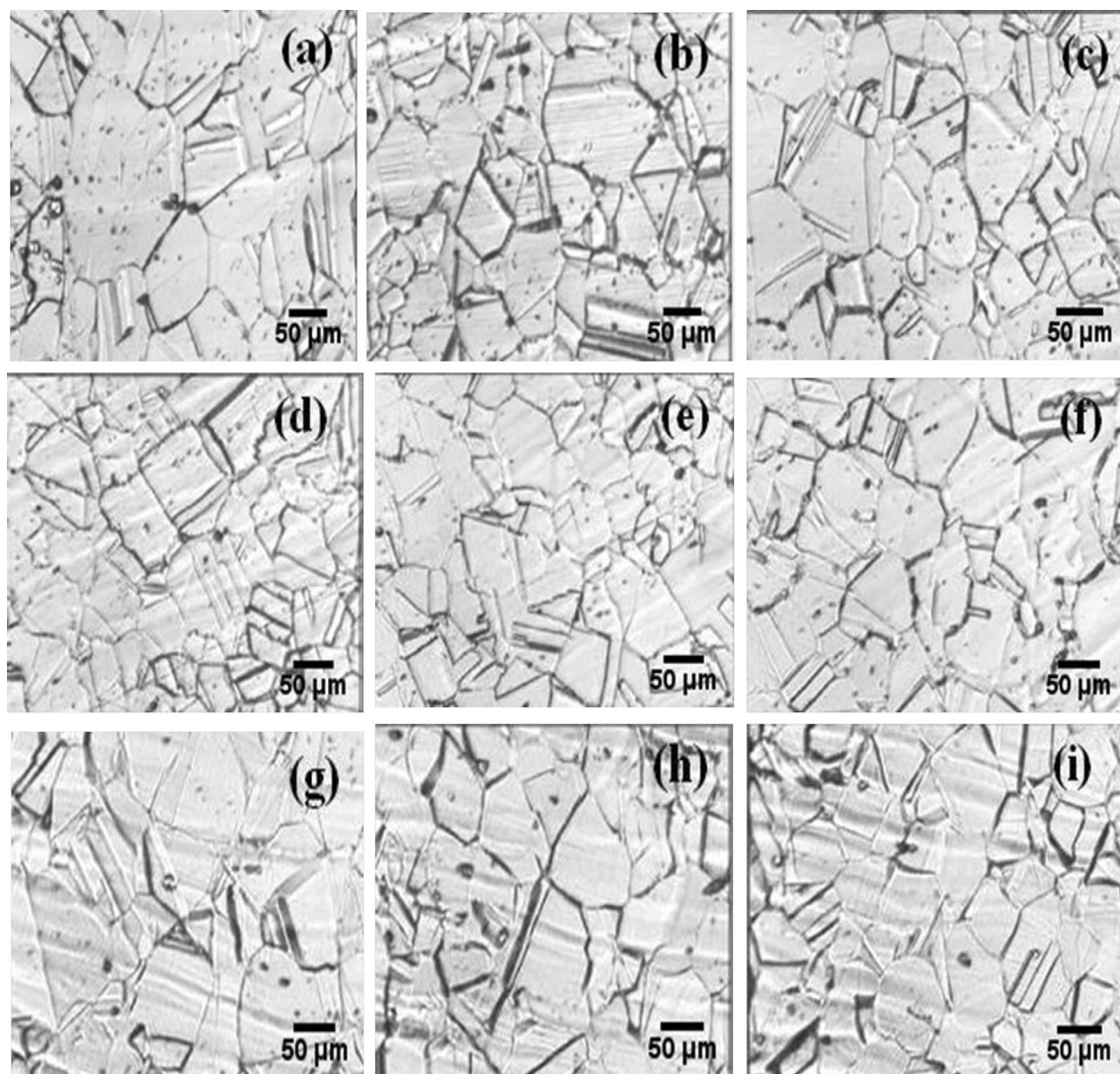


Fig. 8 Optical micrographs obtained as per ASTM A262 Practice A test for the three zones of HAZ. **a–c** 316N1, **d–f** 316N2 and **g–i** 316N3 weldment and **a, d, g** HAZ 1 **b, e, h** HAZ 2 and **c, f, i** HAZ 3

much variation in transpassive potential and all are comparable in as-welded and thermally aged samples as shown in Table 7. Acidic chloride medium is useful to provide the passive film properties, active passive transitions and pitting corrosion susceptibility [37, 38]. Higher the E_{pit} values, better is the pitting corrosion resistance. Figure 9b shows the anodic polarisation curves of as-welded and thermally aged specimens in acidic chloride medium. The values of various electrochemical parameters are given in Table 8. The pitting potential is lowest for the 316N1 specimen among the as-welded and thermally aged specimens as shown in Fig. 9b. In chloride medium as shown in Fig. 9c, it is found that pitting potential of the as-welded samples is higher compared to thermally aged samples. The pitting potential values obtained in 0.5 M NaCl are presented in Table 7. The decrease in pitting potential in

chloride medium compared to acidic chloride medium can be attributed to the presence of SO_4^{2-} ions as these ions shift the pitting potential in nobler direction [8]. In the present study, 316N3 shows the highest pitting corrosion resistance compared to 316N1 and 316N2 due to high N + Cr + Mo content in the weld and in the absence of sensitisation. It is found that from Table 3, N + Cr + Mo content is higher for 316N3 (21.4) compared to N + Cr + Mo in 316N1 (18.34) and 316N2 (20.15). The increase in pitting potential with an increase in N + Cr + Mo can be attributed to the increase in passivity or passive potential range of the film as shown in Table 9. As shown in Tables 8 and 9, there is not much variation in pitting potential among the fusion zone and weldments. Pitting corrosion of metal involves three stages: (1) passive film breakdown (2) metastable pitting and (3) pit initiation

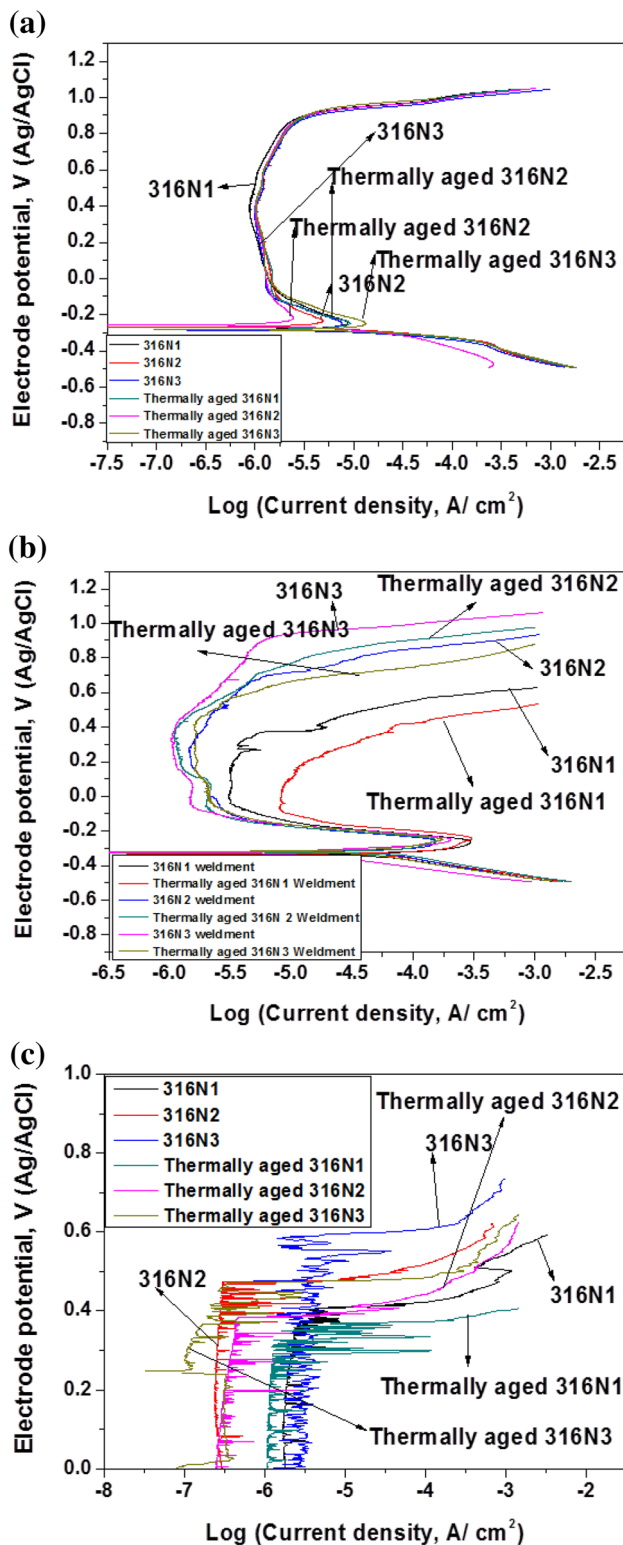


Fig. 9 a Polarisation curves for 316N weldments in the as-welded and thermally aged condition in 0.5 M H₂SO₄ solution. b Polarisation curves for 316N weldments in the as-welded and thermally aged condition in 0.5 M H₂SO₄ + 0.5 M NaCl solution. c Polarisation curves for 316N weldments in the as-welded and thermally aged condition in 0.5 M NaCl solution

and growth. Pitting potential is the potential at which pit growth starts and current increases monotonically with further increase in potential. The metastable pitting and repassivation occur below pitting potential and depend on alloy composition followed by pit growth. All these factors influence the passivity of SS [20, 38]. Thus, as shown in Fig. 9c, metastable pit's growth is retarded with an increase in N + Cr + Mo, and passivity or passive range as shown in Tables 8 and 9 also increases with increase in N + Cr + Mo. These results are in good agreement with the results obtained by several authors [20]. As shown in Figs. 10, 11 and 12, fully grown pit shows preferential attack at austenite centres leaving the ferrite uncorroded. Breakdown of the passive film depends on Cr and Mo, and austenite phase having Cr- and Mo-depleted austenite centres [39] is susceptible to break down of the passive film compared to ferrite which is Cr- and Mo-enriched, and this is a common feature in welds and reported by several authors [39]. As shown in Figs. 10a, b, 11a, b, 12a, b, undissolved ferrite and dissolution of austenite centres are clearly evident indicating that breakdown of passive film has occurred at Cr- and Mo-depleted regions [5, 39]. These observations are in good agreement with previous observations [5]. Polarisation resistance is a useful parameter that gives the information of corrosion characteristic and tendency of a material to undergo corrosion uniformly [20]. Linear polarisation graphs obtained in acidic chloride solution are shown in Fig. 13. From the current density vs electrode potential of LPR graph, as shown in Fig. 13, polarisation resistance is determined from the inverse of slope [40] and is tabulated in Table 10. As shown in Table 10, 316N3 shows higher R_p compared to 316N1 and 316N2. Higher R_p indicates that the material is more corrosion resistant and dissolution of elements is very less. In the present study, 316N3 shows high R_p , indicating that the material is passive in nature and has more passive film stability. This also indicates that the austenite phase in the weld region is more corrosion resistant. As shown in Table 9, the passive film and critical current densities also decreases with increase in N + Cr + Mo along with R_p . All these results indicate the superior corrosion resistance of 316N3. The pitting potential obtained from polarisation experiments correlate well with R_p obtained from LPR technique. The effect of Cr, Mo and N on the pitting corrosion resistance has been studied by several authors, and they have indicated that critical current densities and passive current densities decrease, and pitting potential increases with the increase in these elements [20].

As shown in Table 4, the ferrite number present in the weld after thermal ageing is found to decrease due to the transformation of delta ferrite to carbides, which did not result in sensitisation. As shown in Table 6, the absence of reactivation current or lower values indicates the absence

Table 7 Electrochemical parameters from the anodic polarisation curve for weld metals in 0.5 M NaCl and 0.5 M H₂SO₄

Weld metal identification	Pitting potential, E_{pit} V (Ag/AgCl) in 0.5 M NaCl.	Transpassive potential V (Ag/AgCl) in 0.5 M H ₂ SO ₄
316N1	0.41	0.97
316N2	0.48	0.97
316N3	0.61	0.98
Thermally aged 316N1	0.36	0.96
Thermally aged 316N2	0.42	0.97
Thermally aged 316N3	0.57	0.97

Table 8 Electrochemical parameters from the anodic polarisation curve for weldments in 0.5 M H₂SO₄ + 0.5 M NaCl

Weldment designation	$I_{\text{pass}} \times 10^{-6}$ (A/cm ²) at 0.3 V (Ag/AgCl)	Pitting potential, E_{pit} , V (Ag/AgCl)	OCP
316N1	3.1	0.50 ± 0.05	– 0.34
316N2	1.9	0.73 ± 0.05	– 0.32
316N3	1.0	0.85 ± 0.03	– 0.33
Thermally aged 316N1	5.8	0.42 ± 0.02	– 0.33
Thermally aged 316N2	4.4	0.64 ± 0.02	– 0.33
Thermally aged 316N3	1.17	0.73 ± 0.02	– 0.32

Table 9 Electrochemical parameters from the anodic polarisation curve for weld metals in 0.5 M H₂SO₄ + 0.5 M NaCl

Weld metal identification	$I_{\text{pass}} \times 10^{-6}$ (A/cm ²) at 0.3 V (Ag/AgCl)	Pitting potential, E_{pit} , V (Ag/AgCl)	OCP	$I_{\text{critical CD}} \times 10^{-5}$ (A/cm ²)	Passive range, V (Ag/AgCl)
316N1	8.0	0.45	– 0.34	2.3	0.60
316N2	1.5	0.68	– 0.33	1.3	0.81
316N3	0.8	0.83	– 0.32	0.8	1.04

of sensitisation. In the present study, carbide precipitates formed during welding at 823 K/2 h condition did not result in sensitisation (i.e. Cr content in the depleted zone around carbides more than 13 wt%) and not continuous in nature. Studies carried out on 316N weld metal at 823 K for 4 h show very low DOS values and the presence of carbides that decreases the amount of chromium present near the carbide and hence pitting potential decreases [18]. The micrograph (Figs. 5, 7) show the presence of carbides at austenite/delta ferrite interfaces after thermal ageing in all the weld metals which act as susceptible sites for pit initiation and growth. As shown in Figs. 10c, d, 11c, d, SEM micrographs show undissolved ferrite stringers and dissolution of austenite centres [39] and unattacked carbides. These results indicate that breakdown of passive film occurs at Cr- and Mo-depleted regions and Cr-depleted regions near the carbides which acts as pitting initiation sites.

4 Conclusions

The results of the present study are summarised as follows:

1. ASTM A262 Practice A test at different heat-affected zones of the weldments revealed step structures, indicating the absence of carbide precipitation and sensitisation.
2. Double-loop electrochemical potentiokinetic reactivation test results of the thermally aged weldments of 316N1 showed I_r and degree of sensitisation values as 2.6×10^{-5} and 8.5×10^{-3} , respectively. DLEPR tests on as-welded and thermally aged weldments of 316N2 and 316N3 showed the absence of reactivation peak, confirming the complete absence of sensitisation.
3. The potentiodynamic polarisation studies showed the highest pitting corrosion resistance for 316N3 weldment as compared to 316N2 and 316N1. Pitting corrosion resistance was found to decrease with the thermally aged condition for all the weldments due to

Fig. 10 SEM photograph of as-welded and in thermally aged condition of 316N2 after potentiodynamic polarisation experiment in acidic chloride medium showing dissolution of austenite inside the pit leaving ferrite undissolved **a, b** as-welded condition pit **c, d** in thermally aged condition showing austenite dissolution leaving carbides unattached in pit at lower and higher magnifications

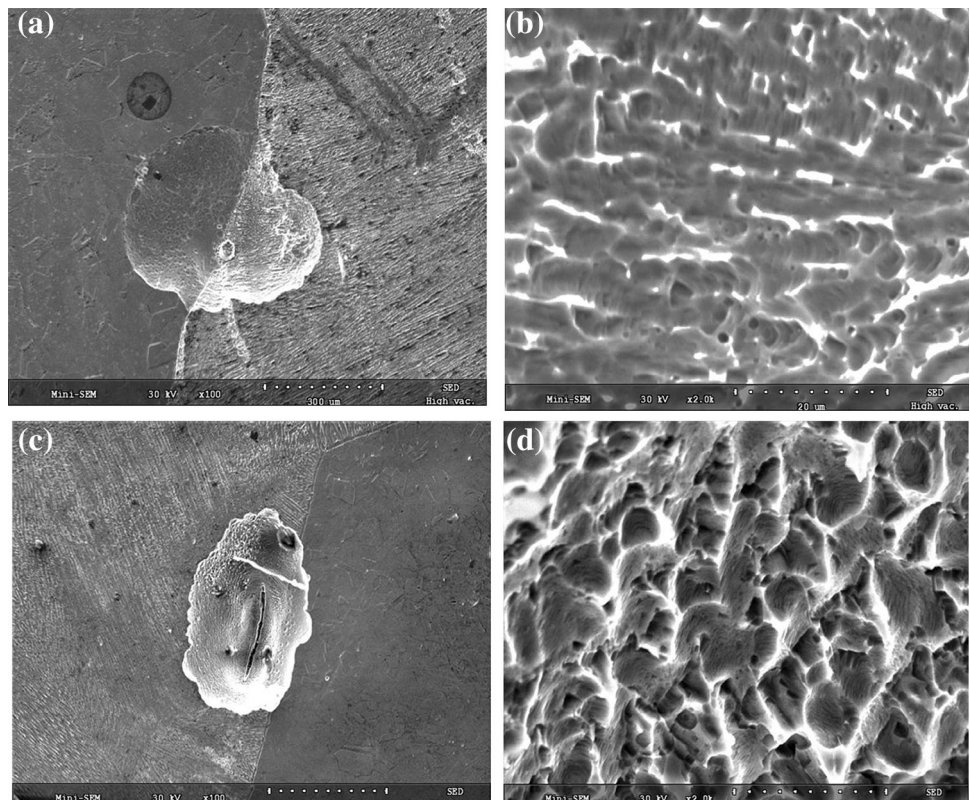


Fig. 11 SEM photograph of as-welded and in thermally aged condition of 316N1 after potentiodynamic polarisation experiment in acidic chloride medium showing dissolution of austenite inside the pit leaving ferrite undissolved **a, b** as-welded condition pit **c, d** in thermally aged condition showing austenite dissolution, leaving carbides unattached in pit at lower and higher magnifications

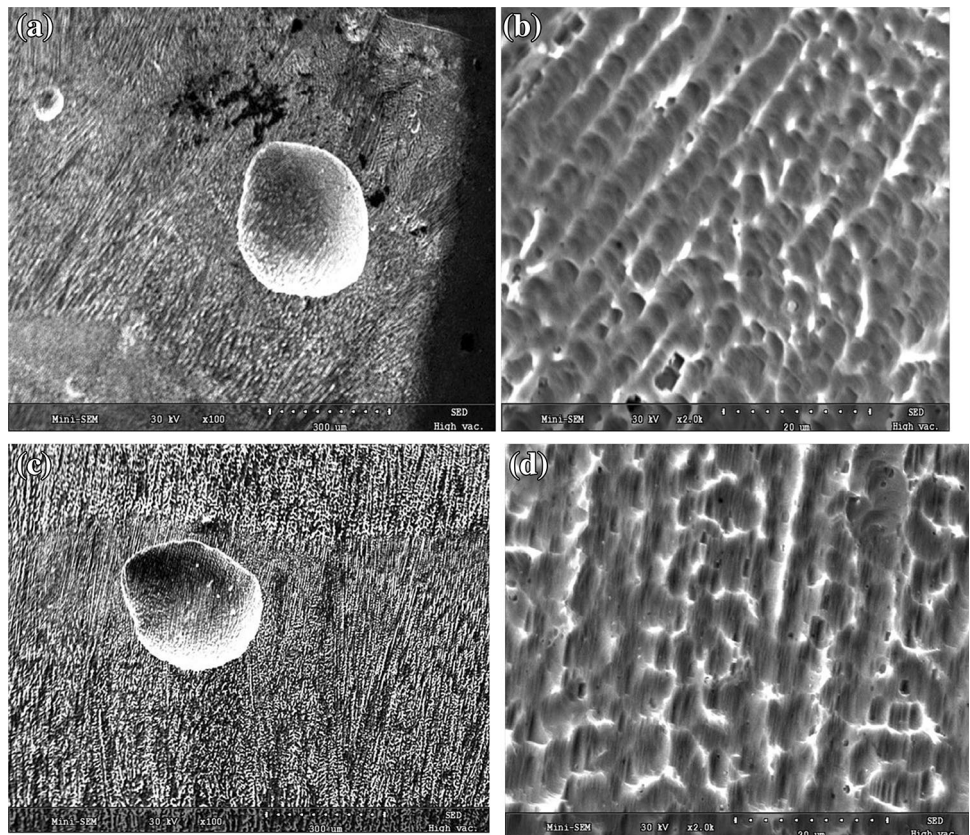


Fig. 12 SEM photograph of as-welded 316N3 after potentiodynamic polarisation experiment in acidic chloride medium showing the dissolution of austenite inside the pit leaving ferrite undissolved **a**, **b** as-welded condition showing austenite dissolution in pit at lower and higher magnifications

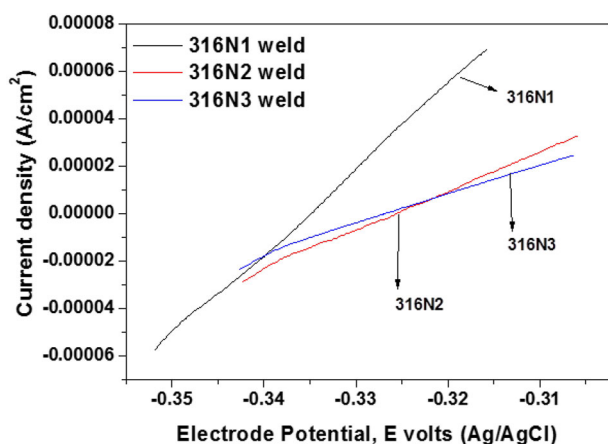
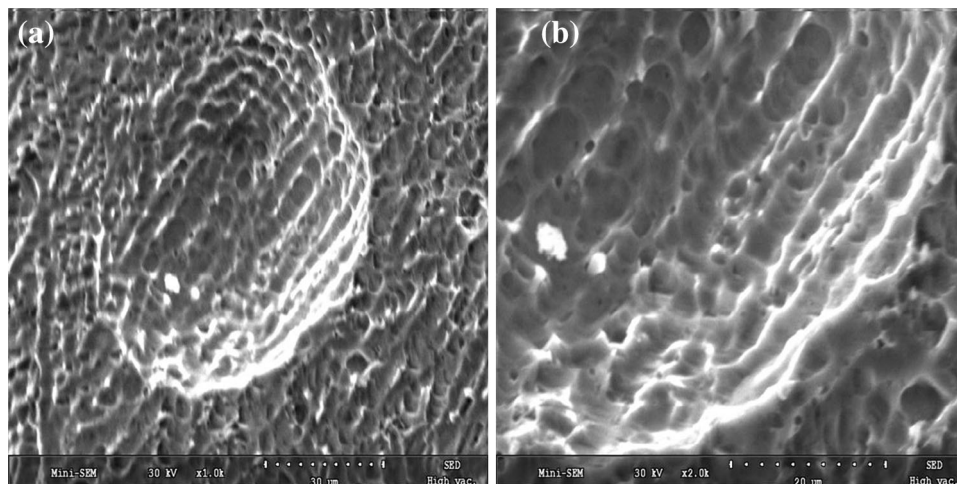


Fig. 13 Linear polarisation experiments for 316N fusion zone in as-welded condition in 0.5 M H_2SO_4 + 0.5 M NaCl

Table 10 Polarisation resistance obtained from linear polarisation experiment for weld metals

Weld metal identification	Polarisation resistance (R_p , Ohm/cm ²)
316N1	281.1
316N2	614.2
316N3	799.3

precipitation of chromium carbides at delta ferrite/austenite interfaces.

- It was found that pitting potential of the as-welded samples was higher in acidic chloride medium compared to sodium chloride medium due to the presence of sulphate ions.
- The polarisation resistance values obtained from the LPR technique increased with the increase in N + Cr + Mo in fusion zone
- Higher pitting potential in 316N3 could be attributed to the presence of higher N + Cr + Mo content in the weld in the absence of sensitisation.

Acknowledgement The authors would like to thank Dr A.K. Bhaduri, Director, IGCAR, for his constant support and encouragement and Smt. P. Sundari, CSTD/MMG, IGCAR, for providing experimental support during the investigation.

References

- Dayal R K, Parvathavarthini N, and Raj B, *Int Mater Rev* **50** (2005) 129.
- Jayakumar T, Bhaduri A K, Mathew M D, Albert S K, and Kamachi Mudali U, *Adv Mater Res* **794** (2013) 670.
- Mannan S L, Chetal S C, Raj B, and Bhoje S B, in Proceedings of Seminar on Materials R&D for PFBR (2013).
- Silva C C, Farias J P, and de Santana HB, *Mater Des* **30** (2009) 1581.
- Kumar S, and Sahi A S, *Int J Comput Appl* **0975-8887** (2015) 1.
- Garcia C, de Tiedra M P, Blanca Y, Martin O, and Martin F, *Corros Sci* **50** (2008) 2390.
- Unnikrishnan R, Idury K S, Ismail T P, Bhandari A, Shekhawat S K, Khatirkar R K, and Sapate S G, *Mater Charact* **93** (2014) 10.
- Pujar M G, Kamachi Mudali U, Dayal R K, and Gill T P S, *Corrosion* **48** (1992) 579.
- Kamachi Mudali U, Hasan Shaikh A R, and Dayal R K, *Intergranular Corrosion Behaviour of Type 316LN Weldments*, NWS (1997) 1.
- Kamachi Mudali U, and Dayal R K, *Mater Sci Technol* **16** (2000) 1.
- Baerlack W A, Savage W F, and Duquette D J, *Weld J Res Suppl* (1979) 83.
- Albert S K, and Bhaduri A K, *Research and Development in Welding and Hard Facing Towards Construction of Prototype Fast Breeder Reactor*, 38th MPA-Seminar, October 1–2, 2012, Stuttgart 195.
- Li L, Chai M, Li Y, Bai W, and Duan Q, *Appl Mech Mater* **331** (2013) 578.
- Vijayanand V D, Laha K, Parameswaran P, Ganesan V, and Mathews M D, *Mater Sci Eng A* **607** (2014) 138.
- Streitner M A, *Theory and Application of Evaluation Test for Detecting Susceptibility to Intergranular Attack in Stainless Steels and Related Alloys-Problems and Opportunities*, ASTM STP 656, American Society for Testing and Material, Philadelphia (1975), p 70.
- Marttilvilpass, *Prediction of Micro Segregation and Pitting Corrosion Resistance of Austenitic Stainless Steel Welds by Modeling*.

- Doctor of Science in Technology Thesis, Helsinki University (1999) p 1–166.
17. Kamachi Mudali U, Dayal R K, Gill T P S, and Gnanamoorthy J B, *Werkstoffe Corros* **37** (1986) 637.
 18. Pujar M G, Parvathavarthini N, Dayal R K, *Mater Chem Phys* **123** (2010) 407.
 19. Toppo A, Pujar M G, Sreevidya N, and Philip J, *Def Technol* **14** (2018) 226.
 20. Poonguzhali A, Pujar M G, and Kamachi Mudali U, *J Mater Eng Perform* **49** (1993) 977.
 21. Ogawa T, Aoki S, Sakamoto T, and Zaizen T, *The Weldability of Nitrogen Containing Austenitic Stainless Steel: Chloride Pitting Corrosion Resistance*. Missouri (1982) p 139.
 22. Ferrar R A, Hulen C, and Thomas R G, *J Mater Sci* **20** (1985) 2828.
 23. Suuatala N, *Metall Trans A* **144** (1983) 191.
 24. Delong W T, *Weld J* **53** (1974) 2735.
 25. Koteck D J, and Siewert T A, *Weld J* **71** (1992) 1715.
 26. Parvathavarthini N, Dayal R K, Kathak H S, Shankar V, and Shanmugan V, *J Nucl Mater* **355** (2006) 68.
 27. Toppo A, Pujar M G, Arivazhagan B, Vasudevan M, Mallika C, and Kamachi Mudali U, *Corrosion* **514** (2016) 295.
 28. Basu K, Das M, Bhattacharjee D, and Chakraborti P C, *Mater Sci Technol* **23** (2007) 1278.
 29. ASTM A262-14, *Standard Practices for Detecting Susceptibility to Intergranular Attack in Austenitic Stainless Steels*, ASTM International, USA (2014).
 30. David S A, *Ferrite Morphology and Variations in Ferrite Content in Austenitic Stainless Steel Welds*, Cleveland, Ohio (1981) p 63.
 31. Takalo T, Suutula N, and Moiso T, *Metall Trans A* **10** (1979) 1173.
 32. Ghosh S K, Jha S, Mallick P, and Chattopadhyay P P, *Mater Manuf Process* **28** (2013) 249.
 33. Aydogdu G H, *Determination of Susceptibility to Intergranular Corrosion in 304L & 316L Type Stainless Steels by Electrochemical Reactivation Method*, Degree of Master of Science Thesis, Middle East Technical University (2004) p 1.
 34. Muraleedharan P, Gnanamoorthy J B, and Prasad Rao K, *Corrosion* **45** (1989) 142.
 35. Parvathavarthini N, and Dayal R K, *J Nucl Mater* **399** (2010) 62.
 36. Mozhi T A, Clark W A T, Nishimoto K, Jhonson W B, and Mac Donald D D, *Corrosion* **41** (1985) 555.
 37. Frankel G S, *J Electrochem Soc* **145** (1998) 2186.
 38. Szklarska-Smialowska Z, *Corrosion* **27** (1971) 223.
 39. Raja V S, *Corros Rev* **21** (2003) 1.
 40. ASTM G102-89, *Standard Practice for Calculation of Corrosion Rates and Related Information from Electrochemical Measurements*, ASTM International, USA, 2014.

Publisher's Note Springer Nature remains neutral with regard to jurisdictional claims in published maps and institutional affiliations.